RSC Advances

PAPER

Cite this: *RSC Adv.*, 2020, **10**, 6213

Bi-functional silica nanoparticles for simultaneous enhancement of mechanical strength and swelling capacity of hydrogels

Majharul Islam Sujan,[a] Stephen Don Sarkar,[a] Salma Sultana,[a] Labiba Bushra,[a] Rizwan Tareq,[ab] Chanchal Kumar Roy[a] and Md. Shafiul Azam *[a]

A combination of strong load-bearing capacity and high swelling degree is desired in hydrogels for many applications including drug delivery, tissue engineering, and biomedical engineering. However, a compromising relationship exists between these two most important characteristics of hydrogels. Improving both of these important properties simultaneously in a single hydrogel material is still beyond the satisfactory limit. Herein, we report a novel approach to address this problem by introducing a silica-based bi-functional 3D crosslinker. Our bi-functional silica nanoparticles (BF-Si NPs) possess amine groups that are able to offer pseudo-crosslinking effects induced by inter-cohesive bonding, and acrylate groups that can form conventional covalent crosslinking in the same hydrogel. We fabricated polyacrylic acid (PAc-Si) and polyacrylamide (PAm-Si) hydrogels using our BF-Si NPs *via* free radical polymerization to demonstrate this concept. Incorporation of the BF-Si crosslinkers into the hydrogels has resulted in a large enhancement in the mechanical properties compared to conventional hydrogel crosslinked with *N*,*N*′-methylene bisacrylamide (MBA). For instance, tensile strength and the toughness increased by more than 6 times and 10 times, respectively, upon replacing MBA with BF-Si in polyacrylamide hydrogel. Moreover, the hydrogels crosslinked with BF-Si exhibited a remarkably elevated level of swelling capacity in the aqueous medium. Our facile yet smart strategy of employing the 3D bi-functional crosslinker for combining high swelling degree and strong mechanical properties in the same hydrogels can be extended to the fabrication of many similar acrylate or vinyl polymer hydrogels.

Received 15th November 2019
Accepted 4th February 2020

DOI: 10.1039/c9ra09528d

rsc.li/rsc-advances

Introduction

Hydrogels are 3D crosslinked hydrophilic polymer networks with the capacity to absorb water or aqueous fluid, thousands of times their polymer network weight.[1] Synthetic hydrogels, similar to biological tissues, are generally fragile and inclined to fracture at small elongation when a nominal force is applied.[2] Such simultaneous solid–liquid dual properties have made hydrogels suitable candidates as raw materials in many applications such as tissue engineering,[3] chemical and bio-sensing,[4] drug delivery,[5] separation technology,[6] *etc.* The applications of hydrogels are frequently derived from the reversible stimuli responsiveness through volume change or phase transition by different physical and chemical stimuli that include electric field, magnetic field, temperature, pH, and ionic strength.[7,8]

Among the stimuli-responsive polymeric hydrogels, polyacrylic acid (PAc) and polyacrylamide (PAm) have been widely studied and have the potential for numerous practical applications.[9] Both of the polymers absorb water and swell due to their hydrophilic nature and crosslinked structure, which make them suitable for biological applications. Being polyanionic (polyacrylic acid), PAc has been extensively used in designing pH-sensitive macromolecular architectures for targeted drug delivery. The pK_a value of PAc lies in between 4.5 and 5.0 which ensures high ionization of the carboxylic acid groups at the physiological pH of 7.4 resulting in an excessive amount of swelling.[10] PAm hydrogels, on the other hand, have drawn immense attention from researchers especially because of their thermal responsiveness.[11] The sol–gel transition of the thermoresponsive hydrogels is triggered by any change in the temperature. For instance, the aqueous solutions of PAm or similar thermoresponsive hydrogels are liquid at ambient temperature and form a gel at physiological temperature, the behavior that leads to their uses in many biomedical and drug delivery applications.[9,12]

Mechanical strength and degree of swelling are the two most critical properties of stimuli-responsive hydrogels that govern their practical applications.[13–15] Extensive works have been done in the last two decades to modify these properties of hydrogels. Several approaches have been successfully implemented to

[a]*Department of Chemistry, Bangladesh University of Engineering and Technology (BUET), Dhaka 1000, Bangladesh. E-mail: mdshafiulazam@chem.buet.ac.bd; azam@ualberta.ca*

[b]*Department of Materials and Metallurgical Engineering, Bangladesh University of Engineering and Technology (BUET), Dhaka 1000, Bangladesh*

obtain mechanically robust hydrogels in the forms of topological,[16] nanocomposite,[17,18] and double-network hydrogels,[19] *etc.* Organic crosslinkers are frequently used to obtain mechanically strong hydrogels, where covalently bonded crosslinkers can play the role of ensuring the structural integrity of hydrogels. On the other hand, the use of a large amount of loosely bonded polyelectrolytes is a way of achieving a hydrogel with a high swelling degree. In the presence of a small amount of crosslinker or weak crosslinking, osmotic pressure can play a role in increasing the volume of hydrogels.[20] Mechanical strength and the swelling capacity show an inverse or compromising relationship with the addition of conventional covalently bonded crosslinker like *N*,*N*′-methylenebisacrylamide (MBA). If strong mechanical properties are achieved in the presence of a large amount of MBA, it has to compromise on the degree of swelling. Interestingly, a high swelling degree is required for many hydrogels without compromising on the mechanical properties for different kinds of applications. However, this kind of research approach is rare in literature. Only one such work is available to the best of our knowledge, where Liu *et al.* introduced a pufferfish-inspired device by encapsulating superabsorbent hydrogel into a mechanically strong hydrogel membrane for achieving a high swelling degree and long-term robustness.[21] However, the process for obtaining such kind of device seems to be complicated as they used laser cutting to introduce uniform pores for water permeation into the hydrogel.

Herein, we develop silica-based crosslinkers capable of forming both conventional covalent crosslinking as well as pseudo-crosslinking for simultaneous enhancement of mechanical properties and swelling degree. The covalent bonds are capable of maintaining the structural integrity of hydrogels during deformation and the weak adhesive type pseudo-bonds such as hydrogen bonding and van der Waals forces are responsible for high degrees of freedom required for swelling. Silica-based nanoparticles have attracted huge attention of the researchers as inorganic fillers for the nanocomposite hydrogels due to their high availability, tunable nanoscale size, and stability in aqueous solution.[22,23] Smart and well-designed functionalization strategies of the inner and outer surfaces of these particles are readily achievable for the desired applications and adequate stability of the Si NPs in aqueous solutions because of their significantly reduced dissolution rate.[24] Moreover, silica particles enhance physical contact and stress transfer among the filler particles and hydrophilic polymer chains owing to their hydrophilic nature and large surface area.[25] For the purpose of obtaining the desired properties, we functionalize silica nanoparticles with a comparable surface concentration of acrylic and amine groups for covalent and pseudo-crosslinking, respectively. Silica crosslinked PAc (PAc-Si) and PAm (PAm-Si) polymeric hydrogels are then synthesized by incorporating the as-synthesized BF-Si NPs as crosslinkers. The mechanical and swelling properties of PAc-Si and PAm-Si hydrogels with variable degrees of crosslinking have been investigated. Moreover, the influences of some stimuli such as pH and temperature on the swelling properties of the as-synthesized hydrogels are discussed.

Experimental

Materials

Tetraethylorthosilicate (TEOS), methacrylic anhydride, (3-aminopropyl)triethoxysilane (APTES) and *N*,*N*′-methylenebisacrylamide (MBA) were purchased from Sigma-Aldrich. Ammonia solution (25%), ethanol, acetone, toluene and *N*,*N*-dimethylformamide (DMF) were collected from Merck, Germany. Acrylic acid and acrylamide monomers were obtained from Loba Chemie, India. The initiator of polymerization potassium persulfate (KPS) was obtained from BDH Chemicals. All the chemicals were used as purchased and deionized (DI) water was used for all experiments.

Synthesis of silica nanoparticles (Si NPs)

A modified Stöber's method was applied to synthesize the silica nano-particles.[26–28] Briefly, 2.9 mL (0.93 g mL^{-1}) of TEOS was dissolved in 20 mL (0.79 g mL^{-1}) of ethanol. Separately, 0.55 mL (0.91 g mL^{-1}) of ammonium hydroxide and 2.9 mL of water were mixed with 23.7 mL of ethanol. Then the two solutions were mixed together in a round bottom flask and stirred for 24 h at room temperature. The obtained silica nanoparticles (Si NPs) in the solution were then collected by centrifugation and dried in a vacuum dryer overnight.

Synthesis of acrylic functionalized silica crosslinker (BF-Si NPs)

Acrylic functionalized silica (BF-Si NPs) crosslinker was synthesized by functionalizing silica nanoparticles (Si NPs) with $-CH{=}CH_2$ groups following a two-step process. The Si NPs obtained from the Stöber's method were first dispersed in a mixture of 120 mL DMF and 80 mL toluene. The dispersed mixture was placed in a round bottom flask where 10 mL of APTES was added under magnetic stirring. The stirring of the solution was continued for 24 h and then the amine-functionalized silica nanoparticles (Am-Si NPs) were separated by centrifugation. Next, the Am-Si NPs were washed in toluene for several times and dried under vacuum dryer for 2 h. The Am-Si NPs were then dispersed in 50 mL of toluene and heated at 120 °C until half of the solution was evaporated off to ensure complete removal of any water. The solution was then cooled down to the room temperature and 4 mL of methacrylic anhydride was added under magnetic stirring that continued another 8 h. The desired BF-Si NPs crosslinkers were then washed several times with acetone and finally vacuum dried in an oven at 60 °C.

Synthesis of PAc-Si and PAm-Si hydrogels

Both PAc-Si and PAm-Si hydrogels were prepared by free-radical polymerization using BF-Si NPs as crosslinkers. For the preparation of PAc-Si, 2.0 g of acrylic acid monomer and variable amounts of crosslinker (0.05, 0.1, 0.3 wt%, with respect to monomer) were dispersed ultrasonically in water (volume of the mixture was 3 mL) for 20 minutes under N_2 atmosphere. Subsequently, 1 mL aqueous solution of initiator containing

10 mg KPS was added to the dispersion and polymerization was carried out at 65 °C for 5 h with magnetic stirring under N_2. During all synthesis total volume of polymerization solution was kept 4 mL. PAm-Si hydrogel was synthesized following the same approach except the polymerization time and temperature were 5 h and 70 °C, respectively. For comparison, PAc and PAm hydrogels were prepared using MBA (0.3 wt% with respect to monomer) as the replacement of our synthesized BF-Si crosslinker.

Analytical instruments and characterization

The infrared spectra were collected in order to verify the modification of Si NPs and the dispersion of it into the hydrogels by employing a Fourier transform infrared (FT-IR) spectrometer (Shimadzu, Japan). After freeze-drying, hydrogels and the other solid samples were grinded and taken a small portion to mix with KBr (Sigma Aldrich, Germany). Sample pellets were made by employing a hydraulic press and the infrared beam was applied on the sample and data was recorded in the frequency range of 400–4000 cm^{-1}. The chemical bonding states of Am-Si and BF-Si NPs were identified using surface-sensitive X-ray photoelectron spectroscopy (XPS: Kratos Analytical, UK). During spectrometer operation, Al-Kα monochromatic radiation was used as the excitation source at a photon energy of 14 keV. XPS peak fitting was accomplished using IGOR Pro software (Wave Metrics, version: 6.04). The surface morphology of the prepared samples was observed by field emission scanning electron microscope (FE-SEM: JEOL, JSM, 7600F). Gold was sputtered on the non-conductive hydrogel samples to better image the surface while performing FE-SEM.

Measurement of the swelling ratio of hydrogels

The swelling ratios of PAc-Si, PAc-MBA, PAm-Si, and PAm-MBA hydrogels (0.05 wt% crosslinker, with respect to monomer) were measured as a function of time to understand the kinetics and as a function of respective stimuli (pH and temperature). After freeze-drying, PAc-Si samples were immersed in 500 mL of phosphate buffer solutions of pH 3.0, 5.0, 7.0, 9.0, and 11.0, while weighing at different time intervals up to 24 hours. The temperature-dependent swelling ratio of PAm-Si was recorded in the temperature range of 20 to 80 °C. The swelling ratios of the samples were calculated using the equation, $SR = \left[\frac{W_t - W_d}{W_d}\right]$, where SR is the swelling ratio, W_t is the mass of the swollen hydrogel, and W_d represents the mass of the dry hydrogel.[29]

Study of the mechanical properties

Tensile stress–strain measurements for all as-prepared hydrogels were carried out on cylindrical samples (10.0 ± 0.1 mm in diameter and 12.0 ± 0.1 mm length) using a universal testing machine (UTM, TestResources, Model 100-P-250-12) at room temperature. The crosshead speed was set at 10.0 mm min^{-1}. The tensile stress (σ) of the hydrogels was recorded from the force data whereas the strain (%) was calculated from the ratio of the length change (Δl) and initial length (l). The Young's modulus was determined from the slope of the stress–strain curves at the initial 10% deformation. The toughness of each specimen was also finalized from the area under the stress–strain curves.

Results and discussion

Silica or silica-based nanoparticles are widely used as fillers in the fabrication of nanocomposite hydrogels for the enhancement of mechanical strength.[30] We employed Stöber method to prepare Si NPs from TEOS.[26,31] TEOS was hydrolyzed in ethanol with aqueous ammonium hydroxide as a catalyst. Si NPs with uniform size and shape were expected to form in this process for the preferential adsorption of residual TEOS over the surface of particles.[32] Si NPs can be easily modified with new functionalities simply *via* silane coupling leading to new properties introduced in the particles.[33,34] Instead of using Si NPs as fillers, we functionalized them with the amine and acrylic groups and used them for crosslinking the polymer chains. A general scheme illustrating the modification of silica has been depicted in Fig. 1(a). Firstly, Si NPs were reacted with APTES for amine ($-NH_2$) functionalization (Am-Si NPs). Am-Si NPs were further functionalized partially with acrylic groups leaving a good fraction of the $-NH_2$ groups unreacted. Consequently, the Si NPs end up having 1 : 1 ratio of the acrylic groups that participate in free radical polymerization and $-NH_2$ groups that are capable of forming noncovalent bonds with the functional groups on the hydrocarbon backbone of the polymer chain. Moreover, the high density of the surface functional groups ($-NH_2$ and vinyl groups) on the silica surface will ensure elevated polymer crosslinking.[35]

The morphology and the particle size distribution of the as-synthesized Si NPs and BF-Si NPs were analyzed from the FE-SEM images as shown in Fig. 1. It was observed that the as-synthesized Si NPs (Fig. 1(b)) were uniform in size and spherical in shape. The FE-SEM micrograph of BF-Si NPs (Fig. 1(c)) showed similar spherical nanosphere, demonstrating that no significant changes in the shape of the particles took place during the functionalization process. The size distribution histograms of both samples are given in Fig. 1(d) and (e). Both Si NPs and BF-Si NPs exhibited narrow particle size distribution, ranging from 30 to 70 nm. However, a slight increase in the average particle size obtained from the Gaussian distribution, from 45 ± 12 nm for Si NPs to 48 ± 14 nm for BF-Si NPs, might be attributed to the functionalization of silica.

FTIR spectroscopy was carried out to investigate the structural changes of Si NPs during the modification with APTES and methacrylic anhydride and the spectra are shown in Fig. 2. The absorption bands at 1090 and 3400–3500 cm^{-1}, indicated by vertical dashed lines in Fig. 2, stand for the asymmetric vibrations of Si–O and O–H/N–H respectively, for all three nanoparticles namely Si NPs, Am-Si NPs, and BF-Si NPs. The asymmetric and symmetric vibrations of the in-plane Si–OH originated bands were observed at 950 and 795 cm^{-1}, respectively. Two intense and broad bands appeared at ~1080–1100 cm^{-1} and ~1200 cm^{-1} were assigned, respectively to the

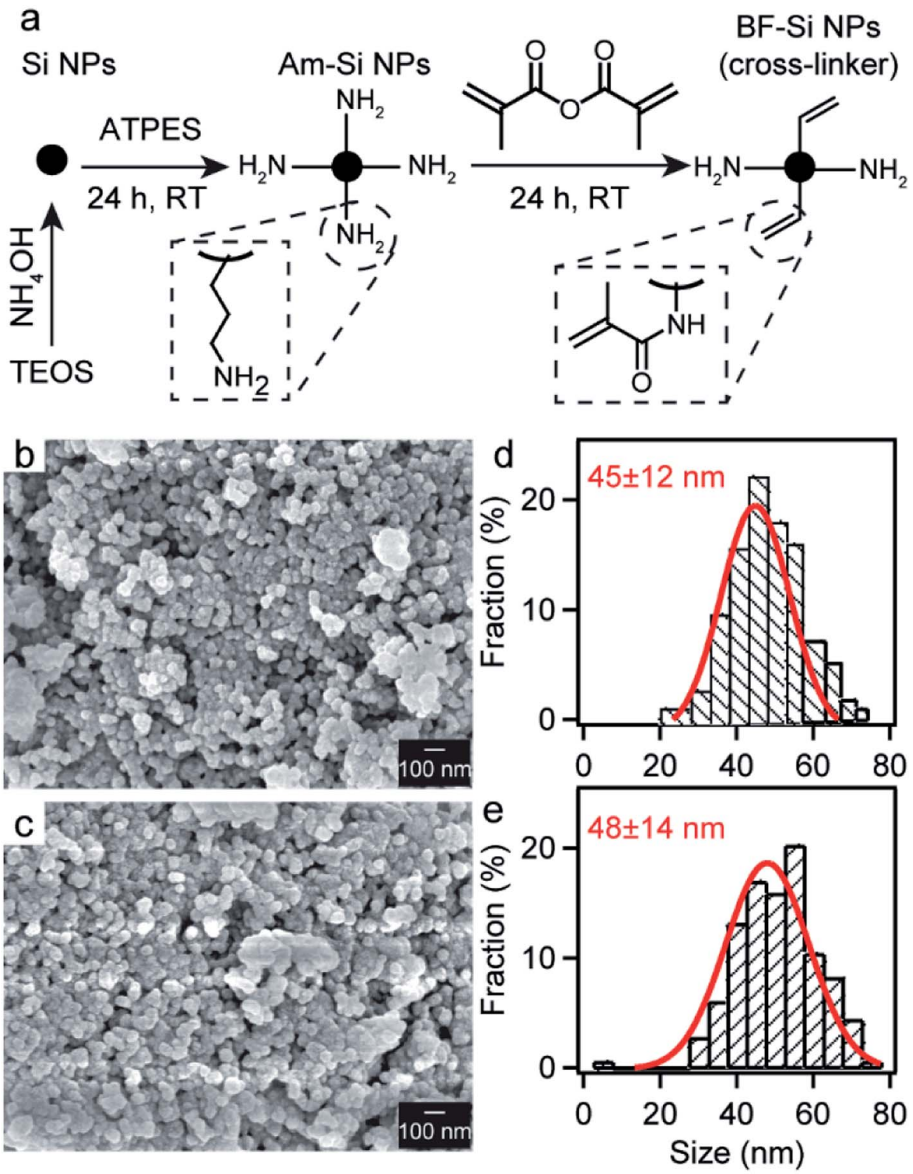

Fig. 1 Schematic illustration of the preparation of BF-Si crosslinker from TEOS (a). FE-SEM images of as-synthesized (b) Si NPs and (c) BF-Si NPs. Particle size distribution histograms of (d) Si NPs, and (e) BF-Si NPs; the red lines show the Gaussian fitting of the respective size distributions.

transversal optical and longitudinal optical modes of the Si–O–Si asymmetric stretching vibrations. Other small peaks as appeared were caused by the surface Si–OH and the residual organic groups.[36] After the modification of Si NPs by APTES, the characteristic peaks appeared at 1634 cm^{-1} and 2930 cm^{-1} were attributed to the N–H bending from primary amine and C–H stretching respectively.[37] Afterward, a further modification to obtain BF-Si NPs was confirmed by the appearance of a peak at 1655 cm^{-1} for the C=O bond of the amide group.[38] Another stretching vibration peak also appeared at 2931 cm^{-1} due to the presence of C–H bonding visible for both Am-Si and BF-Si NPs.

Both samples of Am-Si NPs and BF-Si NPs were also analyzed using the surface sensitive XPS to observe the chemical bonding of the functionalized silica surface. Fig. 3 represents the high-resolution C 1s XPS spectra of Am-Si and BF-Si NPs. The high-resolution C 1s spectrum of Am-Si NPs can be deconvoluted into two different peaks, C–C/C–Si and C–N at binding energy 284.7 eV and 286.3 eV, respectively.[39,40] After the functionalization of Am-Si NPs with methacrylic anhydride, a new peak for N–C=O was found at binding energy 288.4 eV.[41,42] To identify the reaction yield of the functionalization of Am-Si NPs with acrylic group, we carefully observed the peak areas that correspond to the C–N (representative of $–NH_2$ at Am-Si) and N–C=O (representative of –CONH– at BF–Si) groups. The relative percentage of the functional groups calculated from the peak areas of the respective bonds are summarized in Table 1. The relative percentages of C–N and NC=O after the treatment with methacrylic anhydride were found approximately equal indicating ~47% of the surface $–NH_2$ groups converted into acrylamide. The appearance of a new peak for N–C=O in the C 1s

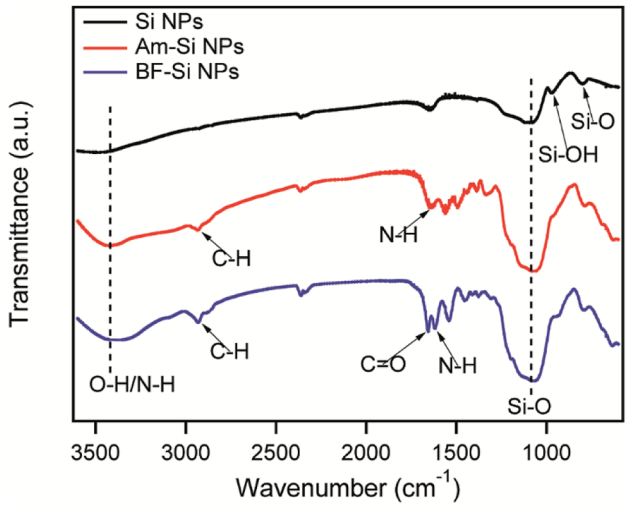

Fig. 2 FTIR spectra of Si NPs (black), Am-Si NPs (red), and BF-Si NPs (blue).

region with a similar percentage of C–N bonds indeed confirmed that our modification of Si NPs resulted in bi-functionality with a comparable density of amine and acrylic groups on the surface.

Next, we synthesized the BF-Si NPs crosslinked polymeric PAc-Si and PAm-Si hydrogels using a one-step polymerization technique. Synthesis routes of PAc-Si NPs and PAm-Si NPs hydrogels are sketched in Scheme 1. The polymerization, we propose here using the BF-Si crosslinkers offers an effective way of tethering the polymer chains around the silica particles leading to a chunk of the hydrogel. The structures and morphologies of the as-synthesized PAc-Si and PAm-Si hydrogels were imaged by FE-SEM microscopy as shown in Fig. 4(a) and (b). In both cases, some spherical or semi-spherical chunks were formed with average diameters of 400–700 nm and 200–400 nm for PAc-Si and PAm-Si, respectively. These observations

Table 1 Percentages of the functional groups obtained from the XPS C 1s peak fitting along with their corresponding binding energies for Am-Si NPs and BF-Si NPs

Materials	Functional group	Binding energy (eV)	% of bonds
Am-Si NPs	C–C, C–Si	284.7	68.4
	C–N	286.3	31.6
BF-Si NPs	C–C/C–Si	284.9	52.3
	C–N	286.1	26.1
	N–C=O	288.4	21.6

with SEM images suggested that the hydrogels were nicely formed surrounding the crosslinker BF-Si NPs and remained somewhat agglomerated in the dried state.

FTIR spectra of the PAc-Si and PAm-Si hydrogels are shown in Fig. 4(c) and (d). Asymmetric vibrations for Si–O bonds near ~1110 cm^{-1} suggested the presence of the BF-Si NPs in both of the hydrogels.[36] The IR bands observed at 2960–2920 cm^{-1} and 1475–1445 cm^{-1} are due to the stretching and bending vibrations, respectively, of CH_2 groups. The peak 1717 cm^{-1} corresponding to C=O stretching vibrations, and the broad band at 3300–3500 cm^{-1} represents the OH stretching of the carboxylic acid groups in PAc-Si hydrogel. The doublet appeared at wavenumber 1240 and 1172 cm^{-1} are attributed to the stretching vibrations of C–OH in PAc-Si.[43] Characteristic C=O stretching appeared near 1650 cm^{-1} merged with the N–H bending at 1595 cm^{-1} are for the amide group of PAm-Si.[37,44] The peaks at 3360 and 3180 cm^{-1} correspond to N–H asymmetric and symmetric stretching vibrations of the amide group, respectively.

We investigated the mechanical strength of the as-prepared PAc-Si and PAm-Si hydrogels (0.3% (w/w) BF-Si NPs with respect to monomer) and compared them with that of conventional PAc-MBA and PAm-MBA hydrogels (0.3% (w/w) MBA with

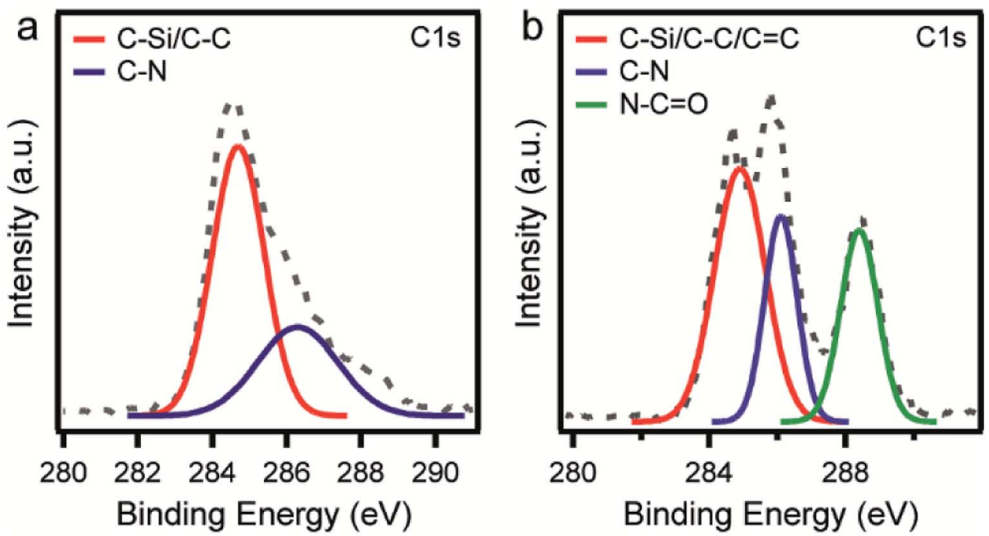

Fig. 3 High-resolution XPS spectra of the C 1s region of (a) Am-Si NPs, and (b) BF-Si NPs.

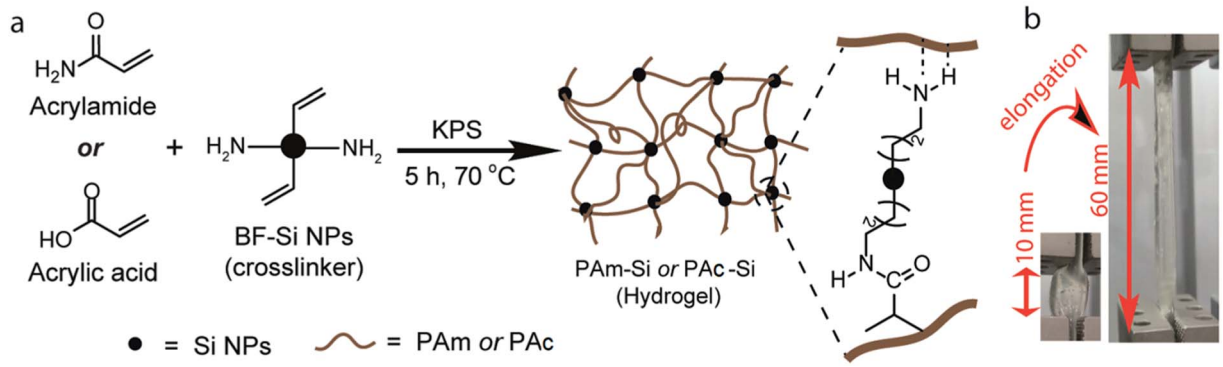

Scheme 1 Schematic illustration of the synthesis of PAc-Si and PAm-Si hydrogels using the as-synthesized BF-Si NPs crosslinker (a). PAc-Si hydrogel before (left) and after (right) 6× elongation (b).

respect to monomer). The tensile tests were performed using a universal testing machine (UTM). The tensile test results are shown in Fig. 5 and the mechanical parameters are summarized in Table 2. It is evident that Young's modulus, tensile strength, elongation at break and toughness of PAc and PAm hydrogels are significantly improved by the incorporation of BF-Si crosslinker compared to the MBA crosslinked hydrogels. The PAc-Si hydrogel with only 0.3% of silica crosslinker could be stretched to more than 17 times its initial length and exhibited toughness 3 times greater than that of the PAc-MBA-0.3% hydrogel. PAm-Si-0.3% hydrogel also demonstrated excellent improvement in toughness and Young's modulus, which were more than 5 times greater than that of the PAm-MBA-0.3% hydrogel. The enhancement of mechanical properties upon crosslinking with BF-Si NPs indicates the strong interaction of the crosslinker with the polymer backbone of hydrogels. BF-Si nanoparticle crosslinker offers two functional sites leading to localized entanglement between the crosslinking sites of the hydrogels, which in turn facilitates the ability of energy dissipation and retards the propagation of cracks.

We observed that the gradual increase of the percentage of BF-Si NPs crosslinker enhanced Young's modulus, tensile strength, elongation at break and toughness in the PAc hydrogels. These observations for PAc-Si suggested that the BF-Si crosslinker not only added structural integrity to the hydrogel by covalent bonds but also favored additional crosslinking interactions that introduced efficient energy dissipation mechanism during the deformation. This additional crosslinking is

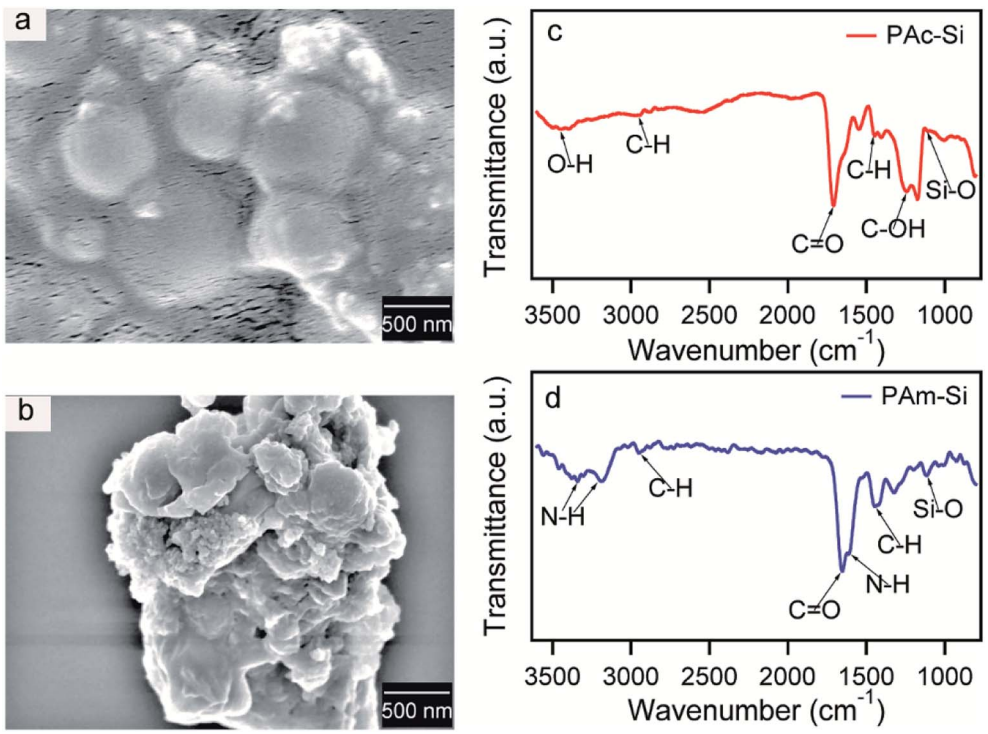

Fig. 4 FE-SEM images of the as-synthesized (a) PAc-Si, and (b) PAm-Si hydrogels. FTIR spectra of (c) PAc-Si, and (d) PAm-Si hydrogels.

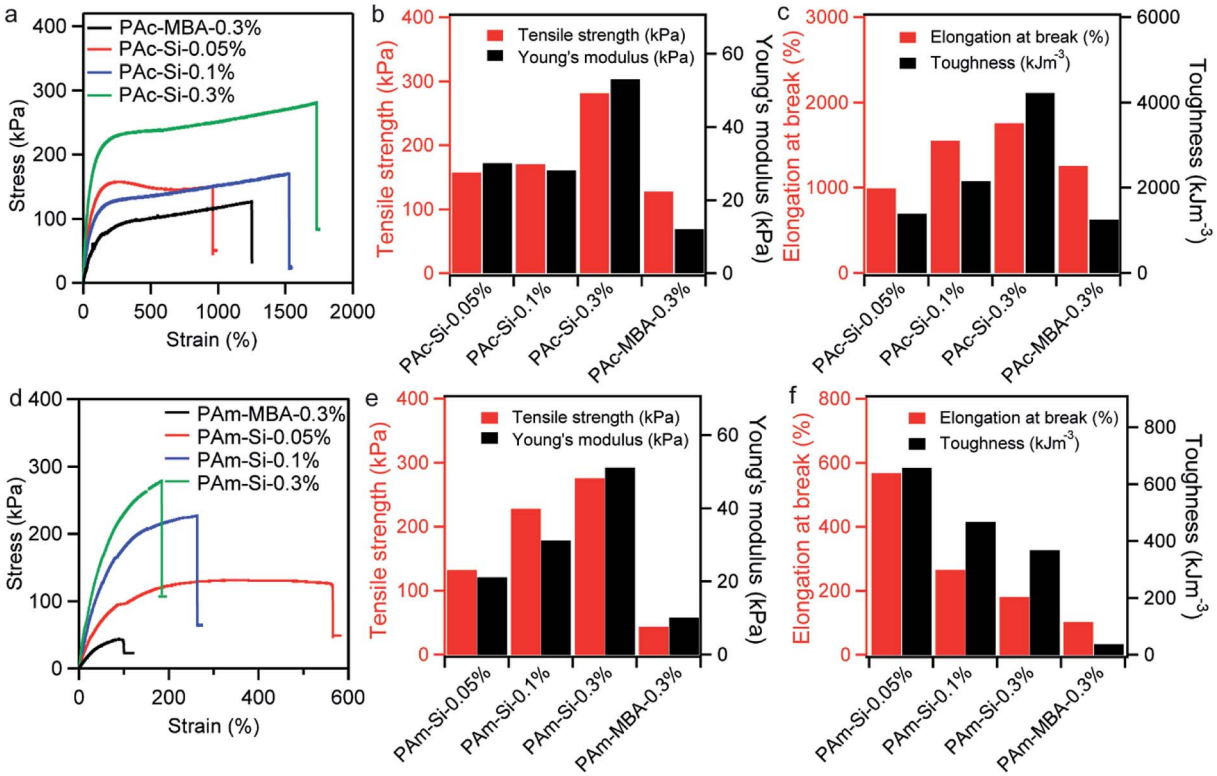

Fig. 5 Mechanical properties of crosslinked polyacrylic acid (PAc) and polyacrylamide (PAm) hydrogels. Tensile stress–strain curves of PAc-Si hydrogels (a) and PAm-Si hydrogels (d) with different ratios of BF-Si NPs (0.05%, 0.1% and 0.3% (w/w) with respect to monomer) and MBA (0.3% (w/w) with respect to monomer). Tensile strength and Young's modulus of crosslinked PAc hydrogels (b) and PAm hydrogels (e), elongation at break and toughness of crosslinked PAc hydrogels (c) and PAm hydrogels (f).

caused by the interim interactions such as mechanical entanglement, hydrogen bonding, hydrophobic bonding, *etc.* besides the actual covalent bonding and is often regarded as pseudo-crosslinking.[45] We hypothesized that the hydrogen bonding between the carboxylic groups of PAc polymer chain and amino functional group on silica contributed to this pseudo crosslinking (Scheme 1). This bi-functionality of BF-Si distinguishes our silica nanoparticle crosslinkers from the conventional chemical crosslinkers. Incorporation of conventional chemical crosslinker such as MBA contributed to the elastic non-dissipative deformation energy of different types of polymeric hydrogels and results in brittle type nature.[46] Here, the introduction of BF-Si crosslinker has enhanced the toughness by the dissipation of viscous energy during the elongation while unaltering the elastic nature (elongation strength) of the PAc and PAm hydrogels. This argument is found in agreement with the reported works by Yang *et al.*[47–49] All the pseudo-crosslinkings of BF-Si are not of a similar type as they differ in bonding energy and entangle types. Sometimes, the pseudo-crosslinking may lead to the formation of a well-ordered structure and densely packed polymer chains in the hydrogels. The SEM image (Fig. 4) of PAc-Si supports the formation of

Table 2 Mechanical properties of the as-synthesized PAm-S hydrogels with variable percentages (w/w, with respect to monomer) of the crosslinker (BF-Si NPs)

Hydrogel	Tensile strength (kPa)	Young's modulus (kPa)	Elongation at break (%)	Toughness (kJ m^{-3})
PAc-Si-0.05%	157	30	987	1385
PAc-Si-0.1%	170	28	1545	2146
PAc-Si-0.3%	281	53	1750	4217
PAc-MBA-0.3%	127	12	1251	1247
PAm-Si-0.05%	131	21	565	655
PAm-Si-0.1%	227	31	263	465
PAm-Si-0.3%	275	51	178	365
PAm-MBA-0.3%	43	10	100	35

well-dispersed polymer chain distribution over the surface of crosslinker leading to the formation of a regular structure. Due to the presence of this kind of packed structure for strong pseudo-crosslinking a large enhancement in mechanical properties in PAc-Si hydrogel has been achieved and increased by the increase in the amount of crosslinker. However, due to the weak interaction energy of the pseudo crosslinking sites of PAm and amino group of the silica surface, a well-aligned and closely packed structure is absent in PAm-Si hydrogel as confirmed by the SEM image and also leads the less prominent enhancement of the mechanical property. We observed that the increase of BF-Si crosslinker to PAm-Si hydrogel increases Young's modulus but caused adverse effects on the toughness and elongation at break. Weak hydrogen bonding or hydrophobic interaction of PAm polymer and the surface of BF-Si crosslinker may be responsible for this kind of temporary interaction.[50]

Many applications of hydrogels like chromatographic packaging and controlled drug release require high swelling capacity in aqueous solution without compromising on the mechanical integrity of the polymeric network.[51] To investigate the swelling capacity of the BF-Si crosslinked hydrogels the swelling ratio of PAc-Si-0.05% and PAm-Si-0.05% hydrogels were examined at different time intervals after immersing in large amount water at pH 7. The swelling ratios of the hydrogels have been plotted against time in Fig. 6(a) and (b). After 15 h both PAc-Si-0.05% and PAm-Si-0.05% hydrogels reached an equilibrium swelling ratio of around 60 ($g\ g^{-1}$) and 25 ($g\ g^{-1}$), respectively. The BF-Si incorporated hydrogels demonstrated a very high equilibrium swelling ratio compared to the corresponding conventional MBA crosslinked hydrogels. The large difference in swelling of PAc-Si-0.05% compared to PAc-MBA-0.05% hydrogel is indicative of differences in the crosslinking mechanism. Usually, PAc hydrogels have high swelling capacity due to the presence of the carboxylic acid group in their polymer backbone, which incur very high osmotic pressure in water. For getting high swelling capacity, PAc hydrogels with a small amount of crosslinker like MBA are preferable.[1,52,53] A small amount of crosslinker gives high degrees of freedom to the polymer backbone to minimize electrostatic repulsion of the carboxylic acid group by absorbing large amounts of water.[54] However, a small amount of MBA in the hydrogel decreases the mechanical strength significantly.[55] Yang *et al.* prepared PAc nanocomposite hydrogel crosslinked by modified Si NPs and obtained significantly improved mechanical performances as obtained with our BF-Si NPs in terms of tensile strength and elongation. However, they observed that the swelling capacity of the reported Si NPs

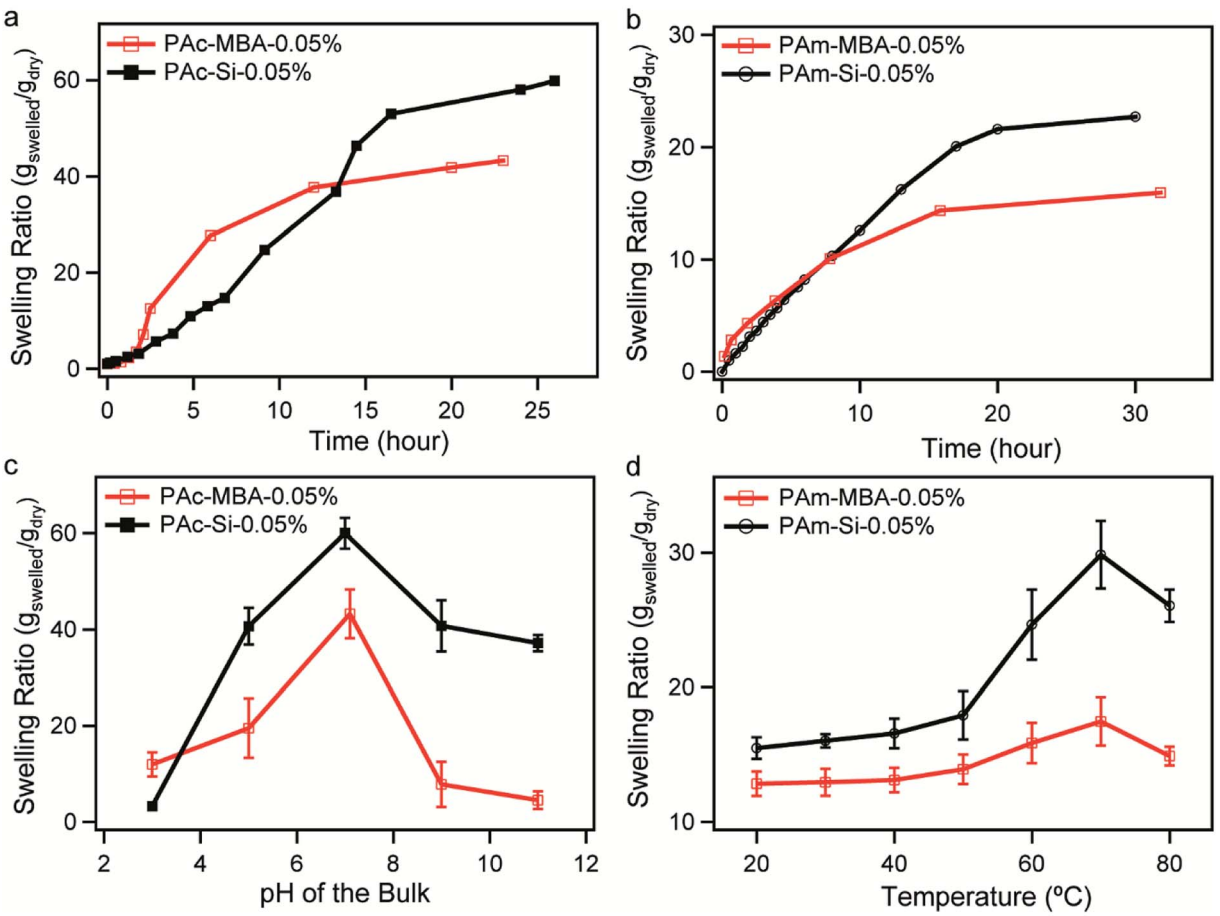

Fig. 6 Time-dependent swelling ratio of PAc (a) and PAm (b) hydrogels. The swelling ratio of PAc hydrogel as a function of pH (c) and swelling degree of PAm hydrogels as a function of temperature (d).

crosslinked hydrogels and MBA crosslinked hydrogel was almost the same showing no enhancement.[48] In the case of PAc-Si, hydrogen bonds between the –COOH groups of polymers and unreacted $-NH_2$ of BF-Si surface render the pseudo-crosslinking effects, which can significantly influence the mechanical strength of the hydrogel network but readily weakens in presence of high dielectric water.[56] The integrity of the hydrogel network is maintained by the covalent crosslinking of nanoparticles and pseudo-crosslinking gives the high degrees of freedom for absorbing large amounts of water. Therefore, a high swelling degree is achieved without the disintegration of PAc-Si hydrogels. However, PAm-Si-0.05% exhibited lower swelling capacity than the PAc-Si-0.05% although the same kind of pseudo-crosslinking is possible for PAm-Si hydrogel. We hypothesize that the non-electrolyte nature of PAm backbone might have been responsible for the lower swelling degree of PAm-Si hydrogel compared to PAc-Si, albeit significantly higher than PAm-MBA.

We investigated the swelling capacity of PAc-Si and PAm-Si hydrogel in response to different stimuli to understand the influence of pseudo-crosslinking on the high swelling degree. pH-dependent swelling for both PAc-Si and PAc-MBA hydrogels confirmed that PAc-Si is more pH-sensitive than PAc-MBA (Fig. 6(c)). The maximum swelling ratio found for PAc-Si (60 (g g^{-1})) was 1.5 times greater than that of PAc-MBA (40 (g g^{-1})) near physiological pH suggesting its potential drug delivery applications. It is worthy to mention here that the swelling ratio declined dramatically after pH 7 for both PAc-Si and PAc-MBA hydrogels. The greater number of ions at higher pH causes dielectric screening of polymer network interaction that results in the collapse of the polymer chain and subsequently reduces the swelling property.[57] The equilibrium and thermal (from 20 to 80 °C) swelling degrees of PAm hydrogels crosslinked with BF-Si and MBA were also investigated as a function of temperature in the range of 20–80 °C (Fig. 6(d)). Usually, conventional PAm hydrogels do not show a very large volume phase transition during swelling in response to thermal stimuli.[58,59] Sometime hydrophobic modification is performed to overcome the limitation.[60] However, our PAm-Si hydrogels exhibited a significant level of volume phase transition during the thermal response. It is indicative of the higher degrees of freedom of polymeric backbone of PAm for absorbing water in presence of BF-Si.

Conclusions

Following a facile strategy, we developed a bi-functional silica crosslinker, which exhibited evidence of forming typical covalent crosslinking and pseudo-crosslinking with polymers such as PAc and PAm. Incorporation of these crosslinkers into hydrogels demonstrated a significant enhancement in the mechanical properties compared to the traditional MBA-crosslinked hydrogels. This enhanced mechanical strength is attributed to the presence of both covalent and noncovalent types of crosslinking in a single hydrogel network. The strong pseudo-crosslinking like hydrogen bonding and other ion–dipole interactions can lead to the dense packing of the polymer chain and thus enhance the mechanical properties. Interestingly, both hydrogels exhibited a high degree of swelling in addition to the enhancement of mechanical strength, which is a rare combination in a single hydrogel. We hypothesized that the pseudo-crosslinking in the hydrogels broke when placed in aqueous media leading to the absorption of large amounts of water without disintegrating the hydrogels. Achieving this rare combination of high swelling capacity and strong mechanical properties in the same hydrogel by simply exploiting a bi-functional crosslinker would benefit many science and engineering researches focused on developing drug carriers, soft-robotics, biomedical devices, and actuators.

Conflicts of interest

There are no conflicts to declare.

Acknowledgements

The authors are thankful to BUET, Ministry of Science and Technology (Government of the People's Republic of Bangladesh), and The World Academy of Sciences (TWAS) for the funding.

References

1 J. E. Elliott, M. Macdonald, J. Nie and C. N. Bowman, *Polymer*, 2004, **45**, 1503–1510.
2 C. Tsitsilianis, *Soft Matter*, 2010, **6**, 2372–2388.
3 M. Pensalfini, A. E. Ehret, S. Stüdeli, D. Marino, A. Kaech, E. Reichmann and E. Mazza, *J. Mech. Behav. Biomed. Mater.*, 2017, **69**, 85–97.
4 I. Y. Jung, J. S. Kim, B. R. Choi, K. Lee and H. Lee, *Adv. Healthcare Mater.*, 2017, **6**, 1601475.
5 P. Treenate and P. Monvisade, *Int. J. Biol. Macromol.*, 2017, **99**, 71–78.
6 P. Calvert, *Adv. Mater.*, 2009, **21**, 743–756.
7 P. Mohammadzadeh Pakdel and S. J. Peighambardoust, *J. Environ. Manage.*, 2018, **217**, 123–143.
8 X. Qi, M. Liu, Z. Chen and R. Liang, *Polym. Adv. Technol.*, 2007, **18**, 184–193.
9 S. Chatterjee and P. C.-l. Hui, in *Hydrogels-Smart Materials for Biomedical Applications*, IntechOpen, 2018.
10 W. Wang and A. Wang, *J. Appl. Polym. Sci.*, 2009, **112**, 2102–2111.
11 G. S. Georgiev, Z. P. Mincheva and V. T. Georgieva, *Macromol. Symp.*, 2001, **164**, 301–312.
12 L. Klouda and A. G. Mikos, *Eur. J. Pharm. Biopharm.*, 2008, **68**, 34–45.
13 A. Dutta, S. Maity and R. K. Das, *Macromol. Mater. Eng.*, 2018, **303**, 1800322.
14 H. Furukawa, K. Horie, R. Nozaki and M. Okada, *Phys. Rev. E: Stat., Nonlinear, Soft Matter Phys.*, 2003, **68**, 031406.
15 H. J. Kong, E. Wong and D. J. Mooney, *Macromolecules*, 2003, **36**, 4582–4588.
16 Y. Okumura and K. Ito, *Adv. Mater.*, 2001, **13**, 485–487.
17 K. Haraguchi, *Curr. Opin. Solid State Mater. Sci.*, 2007, **11**, 47–54.

18 T. Huang, H. G. Xu, K. X. Jiao, L. P. Zhu, H. R. Brown and H. L. Wang, *Adv. Mater.*, 2007, **19**, 1622–1626.
19 J. P. Gong, Y. Katsuyama, T. Kurokawa and Y. Osada, *Adv. Mater.*, 2003, **15**, 1155–1158.
20 H. J. Kwon, Y. Osada and J. P. Gong, *Polym. J.*, 2006, **38**, 1211.
21 X. Liu, C. Steiger, S. Lin, G. A. Parada, J. Liu, H. F. Chan, H. Yuk, N. V. Phan, J. Collins and S. Tamang, *Nat. Commun.*, 2019, **10**, 493.
22 H. Zou, S. Wu and J. Shen, *Chem. Rev.*, 2008, **108**, 3893–3957.
23 B. T. Cheesman, J. D. Willott, G. B. Webber, S. Edmondson and E. J. Wanless, *ACS Macro Lett.*, 2012, **1**, 1161–1165.
24 G. Giovannini, P. Warncke, D. Fischer, O. Stranik, A. J. Hall and V. Gubala, *Nanotoxicology*, 2018, **12**, 407–422.
25 Z. Tai, J. Yang, Y. Qi, X. Yan and Q. Xue, *RSC Adv.*, 2013, **3**, 12751–12757.
26 W. Stöber, A. Fink and E. Bohn, *J. Colloid Interface Sci.*, 1968, **26**, 62–69.
27 S.-H. Wu, C.-Y. Mou and H.-P. Lin, *Chem. Soc. Rev.*, 2013, **42**, 3862–3875.
28 K. Tadanaga, K. Morita, K. Mori and M. Tatsumisago, *J. Sol-Gel Sci. Technol.*, 2013, **68**, 341–345.
29 J. Shen, B. Yan, T. Li, Y. Long, N. Li and M. Ye, *Soft Matter*, 2012, **8**, 1831–1836.
30 J. Yang, F.-K. Shi, C. Gong and X.-M. Xie, *J. Colloid Interface Sci.*, 2012, **381**, 107–115.
31 J. C. Berg, *An introduction to interfaces & colloids: the bridge to nanoscience*, World Scientific, 2010.
32 T. Nakamura, M. Mizutani, H. Nozaki, N. Suzuki and K. Yano, *J. Phys. Chem. C*, 2007, **111**, 1093–1100.
33 Y. Lian, W. Zhang, L. Ding, X. Zhang, Y. Zhang and X.-d. Wang, in *Novel Nanomaterials for Biomedical, Environmental and Energy Applications*, ed. X.Wang and X.Chen, Elsevier, 2019, pp. 241–273, DOI: 10.1016/B978-0-12-814497-8.00008-4.
34 J. S. Sonn, J. Y. Lee, S. H. Jo, I.-H. Yoon, C.-H. Jung and J. C. Lim, *Ann. Nucl. Energy*, 2018, **114**, 11–18.
35 J. Fu, *J. Polym. Sci., Part B: Polym. Phys.*, 2018, **56**, 1336–1350.
36 A. Beganskienė, V. Sirutkaitis, M. Kurtinaitienė, R. Juškėnas and A. Kareiva, *Mater. Sci.*, 2004, **10**, 287–290.
37 I. Ab Rahman, M. Jafarzadeh and C. Sipaut, *Ceram. Int.*, 2009, **35**, 1883–1888.
38 Z. Liu, J. Du, Y. Tan, L. Cao, S. Xu and J. Huang, *Polym. Compos.*, 2018, **39**, 3969–3976.
39 F. Mahnaz, M. Mostafa-Al-Momin, M. Rubel, M. Ferdous and M. S. Azam, *RSC Adv.*, 2019, **9**, 30358–30369.
40 M. S. Islam, N. Akter, M. M. Rahman, C. Shi, M. T. Islam, H. Zeng and M. S. Azam, *ACS Sustainable Chem. Eng.*, 2018, **6**, 9178–9188.
41 J. Guo, K. Song, B. Wu, X. Zhu, B. Zhang and Y. Shi, *RSC Adv.*, 2017, **7**, 22875–22881.
42 H. J. Kim, I.-S. Bae, S.-J. Cho, J.-H. Boo, B.-C. Lee, J. Heo, I. Chung and B. Hong, *Nanoscale Res. Lett.*, 2012, **7**, 30.
43 A. Navaee and A. Salimi, *RSC Adv.*, 2015, **5**, 59874–59880.
44 M. S. Azam, S. L. Fenwick and J. M. Gibbs-Davis, *Langmuir*, 2011, **27**, 741–750.
45 H. G. Nam, M. G. Nam, P. J. Yoo and J.-H. Kim, *Soft Matter*, 2019, **15**, 785–791.
46 J. Maitra and V. K. Shukla, *Am. J. Polym. Sci.*, 2014, **4**, 25–31.
47 J. Yang, L.-H. Deng, C.-R. Han, J.-F. Duan, M.-G. Ma, X.-M. Zhang, F. Xu and R.-C. Sun, *Soft Matter*, 2013, **9**, 1220–1230.
48 J. Yang, C.-R. Han, J.-F. Duan, F. Xu and R.-C. Sun, *Nanoscale*, 2013, **5**, 10858–10863.
49 J. Yang, J.-J. Zhao, C.-R. Han and J.-F. Duan, *Compos. Sci. Technol.*, 2014, **95**, 1–7.
50 N. Sato, Y. Aoyama, J. Yamanaka, A. Toyotama and T. Okuzono, *Sci. Rep.*, 2017, **7**, 6099.
51 S. K. Bajpai, *J. Sci. Ind. Res.*, 2001, **60**, 451–462.
52 L. Carlsson, S. Rose, D. Hourdet and A. Marcellan, *Soft Matter*, 2010, **6**, 3619–3631.
53 J. Shen, B. Yan, T. Li, Y. Long, N. Li and M. Ye, *Soft Matter*, 2012, **8**, 1831–1836.
54 R. Skouri, F. Schosseler, J. Munch and S. Candau, *Macromolecules*, 1995, **28**, 197–210.
55 W. Hu, Z. Wang, Y. Xiao, S. Zhang and J. Wang, *Biomater. Sci.*, 2019, **7**, 843–855.
56 Á. Serrano-Aroca, *Hydrogels*, 2018, 91.
57 D. Chen, L. Wang, Y. Ma and W. Yang, *NPG Asia Mater.*, 2016, **8**, e301.
58 A. A. Abraham and A. K. Sen, *J. Appl. Polym. Sci.*, 2010, **117**, 2795–2802.
59 R. Pelton, *Adv. Colloid Interface Sci.*, 2000, **85**, 1–33.
60 W. J. Peer, in *Polymers in Aqueous Media*, American Chemical Society, 1989, vol. 223, ch. 20, pp. 381–397.

